Journal of the Ceramic Society of Japan 116 [7] 815-821 2008 **Paper**

Conduction properties of non-stoichiometric hydroxyapatite whiskers for biomedical use

Yumi TANAKA,[*,†] Seiko TAKATA,[*,] Kazuki SHIMOE,[*,**] Miho NAKAMURA,[*] Akiko NAGAI,[*] Takeshi TOYAMA[**] and Kimihiro YAMASHITA[*]**

[*]**Department of Inorganic Materials, Institute of Biomaterials and Bioengineering, Tokyo Medical and Dental University, 2–3–10, Kanda-Surugadai, Chiyoda-ku, Tokyo 101–0062**

[**]**Department of Materials and Applied Chemistry, Faculty of Science and Engineering, Nihon University, 1–8–14, Kanda-Surugadai, Chiyoda-ku, Tokyo 101–8308**

Hydroxyapatite (HA) whiskers were synthesized by a hydrothermal method and ion conductive property was investigated in order to develop HA whisker electrets for biomedical utilization. Based on infrared (IR) spectroscopy and inductively coupled plasma optical emission spectrometry (ICP-OES), the obtained whiskers were assumed to be Ca deficient HA with a composition of $Ca_{9.18}[HPO_4]_{0.82}[PO_4]_{5.18}[OH]_{1.18}\cdot n\ H_2O$. The results of complex impedance measurements proved that the conduction properties of whiskers and powders showed almost the same temperature dependence as those of sintered HA above 600°C. The mechanism is understood by the migration of protons originating in OH^- ions. In the temperature range below 600°C, however, the non-linear Arrhenius relationship of conductivity (σ vs. $1/T$) was only observed in the whiskers and powders. In particular, a drastic change in conductivity with temperature appeared in the whiskers within 250–600°C; the conductivity increased to 5.0×10^{-9} S/cm at 500°C, then decreased to 1.7×10^{-9} S/cm with the temperature elevated to 600°C. Since HPO_4^{2-} ions are reportedly supposed to convert into $P_2O_7^{4-}$ in almost the same temperature range where the drastic change in conductivity appeared, the increase in whisker conductivity up to 500°C is presumably the result of an increase in the number of mobile protons generated from HPO_4^{2-}. The subsequent decrease in conductivity seemed to be caused by a decrease in the number of protons achieved by water elimination, causing the conversion of HPO_4^{2-} to $P_2O_7^{4-}$.

Key-words : Hydroxyapatite, Whisker, Bio ceramics, Ion conductivity, Electret, Polarization

[Received February 25, 2008; Accepted April 17, 2008]

1. Introduction

In order to respond to demands in the fields of medical technology, technical innovation is constantly ongoing. We consider that one of the most promising approaches to the innovation is the utilization of biomedical electrets. Since an electret has stable electric fields on its surface, some biological effects are reasonably expected. We previously reported that some types of bioceramics with relatively high ionic conductivity could be turned into electrets under a direct electric field at an elevated temperature.[1),2)] The polarized biomaterials were experimentally proved as new functionalized biomaterials that can actively manipulate biological phenomena. It is also probable that a variety of biomaterials can be subjected to the poling technique because poling is a convenient post-treatment process.

Polarized hydroxyapatite (HA, $Ca_{10}[PO_4]_6[OH]_2$, a well-known artificial bone substitute) is a representative electret, in which the dipoles are formed by a slight shift of the protons in the structure.[3),4)] For dense HA ceramics, we have already reported many actual examples of manipulating biological reaction such as the enhancement of osteoconduction both *in vivo* and *in vitro*.[5)–8)]

Concerning research on HA electrets, we are also considering morphology and stoichiometry. Since HA demonstrates different chemical and mechanical properties depending on the crystal faces in the hexagonal lattice,[9)] the HA whiskers with anisotropic growth orientation usually show, for example, excellent selectivity in the absorption of biological materials and good reinforcement efficiency by mixing with the other biomaterials.[10)] Combining the morphology-based functions with electromagnetic functionalization via the poling treatment is leading researchers to the expectation of expanded applications of HA whiskers. For the control of electromagnetic power on the HA whiskers, however, very little study of the details of the ion conductive properties of the whiskers has been done. This paper deals with the ion conductive properties of HA whiskers from the perspective of comparing HA powders and sintered HA with isotropic growth orientations.

2. Experimental procedure

2.1 Synthesis of HA whiskers and powders

HA whiskers were synthesized via amorphous calcium phosphate (ACP) because large, pure crystals could be obtained when ACP was used as a precursor.[11)] The procedure is briefly described below. ACP was precipitated by pouring 1.0 mol/l $[NH_4]_2HPO_4$ aqueous solution into an equal volume of 0.17 mol/l $Ca[NO_3]_2$ aqueous solution. The pH of the $[NH_4]_2HPO_4$ solution was adjusted to 10.5 by ammonia in advance. After washing and drying, 0.8 g of the ACP powders was ultrasonically dispersed into 24 ml of 1.0 mol/l CH_3COOH aqueous solution and then 12 ml of diluted water was added to it. The prepared ACP suspension was converted into a suspension of HA whiskers under hydrothermal conditions at 210°C for 3 h in a sealed vessel. The ionic ratio of the obtained HA whiskers was analyzed by induc-

† Corresponding author: Y. Tanaka; E-mail: tanaka.bcr@tmd.ac.jp

tively coupled plasma optical emission spectrometry (ICP–OES). Alternatively, HA powders were synthesized by the wet method as follows. CaO powders were converted into a $Ca[OH]_2$ suspension (7.0 mass%) by pouring into decarbonated water. Until the molar ratio of Ca/P reached 1.67, H_3PO_4 aqueous solution (28 mass%) was dropped into the suspension under stirring. After stirring for another several tens of hours, the precipitate was filtered, washed, and dried, resulting in HA powders. The morphology of the synthesized HA whiskers and powders were observed by using a scanning electron microscope (SEM). The crystal structure was identified by 2 θ/θ X-ray diffraction measurement (XRD) using Cu Kα radiation. The conditions of ionic binding were estimated by the results of infrared (IR) spectroscopy. Thermogravimetric analysis was also carried out in order to investigate the thermal water elimination from HA whiskers and powders.

2.2 Ion conductivity measurement

For ion conductivity measurements, HA whiskers and powders were isostatically pressed into compacts (φ 13 mm, thickness 1.0 mm) under a pressure of 150 MPa. For comparison, a dense HA pellet was also prepared by sintering the powder compact at 1250°C for 2 h. During the sintering, water vapor was introduced into the furnace in order to prevent the release of OH^- ions from the HA.

Ion conductivity was estimated by the results of complex impedance measurements of the samples with Pt electrodes. The measurements were carried out in the air in the frequency range of 100 Hz–10 MHz with an applied AC voltage of 0.1 V. The temperature range was from room temperature to 850°C at increments of 5°C/min while 10 min intervals were provided at each measured temperature. The morphology and structural changes with impedance measurements were estimated by SEM, XRD, and IR measurements.

3. Results and discussion

3.1 Characterizations of as-deposited HA whiskers and powders

Figure 1 shows SEM photographs of as-deposited HA crystals synthesized by the hydrothermal treatment of ACP (Fig. 1(a)) and by the wet method (Fig. 1(b)). It is clear that there is large difference in morphology between them: the former consists of large whiskers with an anisotropic aspect of 10–20 μm in length and 1.0–1.5 μm in width, while the latter consists of aggregates of spherical particles with a diameter of 0.2–0.3 μm. In the XRD patterns of as-deposited HA whiskers and powders, all peaks in both are identified as diffractions of HA and there are no obvious differences in the peak positions (**Fig. 2**). The lattice constant was calculated to be $a = b = 9.430$ (6), $c = 6.884$ (4) for the whiskers and $a = b = 9.426$ (4), $c = 6.885$ (2) for the powders, showing that the crystal structure of the whiskers was consistent with that of the powders. However, the peak shapes of the whiskers seemed to be broader than were those of the powders, except for a peak that originated in (002). It was also found that the relative intensity of some peaks such as (002) and (300) was different between the whiskers and powders. The coherent region for XRD diffraction along the *c*- and *a*-axes was estimated by full width half maximum of the peak of (002) and (300) using Scherrer relation; the values obtained were 0.11 μm and 0.04 μm for the whiskers and 0.11 μm and 0.09 μm for the powders. Based on the results, the coherent region along the *c*-axis in the whiskers was about 3 times as large as the region for the *a*-axis. The smaller coherent region and the aspect ratio of whiskers in comparison with those estimated by the SEM observation indicate the aggregation of several numbers of crystalline in one whisker. **Figures 3**A(a) and (b) are IR patterns of the whiskers and powders. In both patterns, the characteristic absorbance that originated in the vibrations of the PO_4^{3-} and OH^- ions in the HA structure was observed. It is generally known that the preparation of pure, large HA whiskers without CO_3^{2-} is difficult.[12),13)] However, judging from the lack of typical absorption by CO_3^{2-} (Fig. 3A(a)), the whiskers in this study were shown to not include any CO_3^{2-}. The peaks that originated in the stretching mode of the P–O bonds and the bending mode of the O–P–O bonds are marked with short solid lines (sharp peaks at about 962 cm^{-1} and broad peaks around 1030–1090 cm^{-1}) and with short dotted lines (peaks at about 470, 560, and 600 cm^{-1}) in the Figs., respectively. Absorbance by the OH^- ions is marked with solid cones; the peaks at about 630 cm^{-1} and 3570 cm^{-1} were attributed to the librational and stretching modes. The good agreement in the positions of the above-described peaks with those reported by Koutsopoulos[14)] suggests that both of the whiskers and powders synthesized in this study have basically the same ionic binding energy in the PO_4^{3-} ion and OH^- ion with that of stoichiometric HA. However IR absorption by the OH^- ions in the whiskers was lower than that in the powders. The relative peak intensity of OH^- libration (630 cm^{-1}) against O–P–O bending (470, 560, and 600 cm^{-1}) was 28.1% for the whiskers and 41.4% for the powders. This fact probably means that the OH^- content in the whiskers is about 68% when the content in the powders is assumed to be 100%. Furthermore, in the case of whiskers, an additional peak and shoulder appeared at around 870 cm^{-1} (see magnified patterns in Fig. 3B) and 1145 cm^{-1}, indicating the presence of HPO_4^{2-} ions in HA. It was reported that absorbance peaks at 962 cm^{-1} and around 1020–1100 cm^{-1} also appeared in the IR pattern if HA includes HPO_4^{2-}.[14)] A little difference in the shapes around the peaks of O–P–O bending between the whiskers and powders is also thought to arise from the presence of

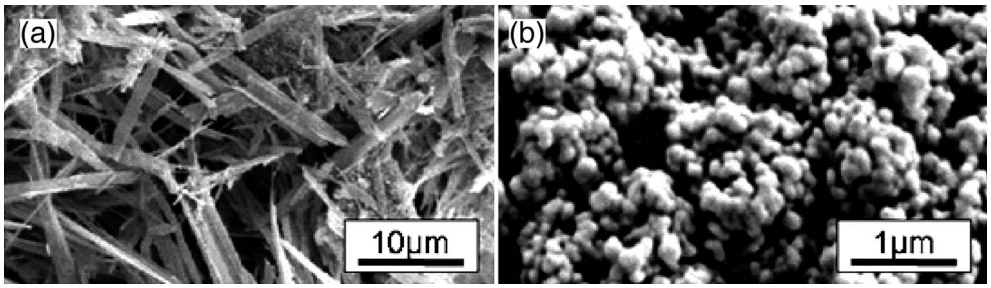

Fig. 1. SEM photographs of as-deposited HA crystalline prepared by (a) hydrothermal method via ACP and (b) wet method.

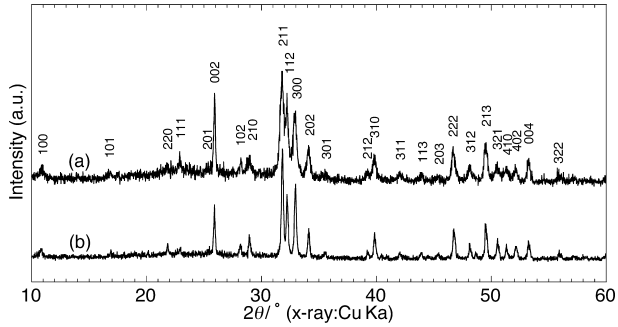

Fig. 2. XRD patterns of (a) as-deposited HA whiskers and (b) as-deposited HA powders.

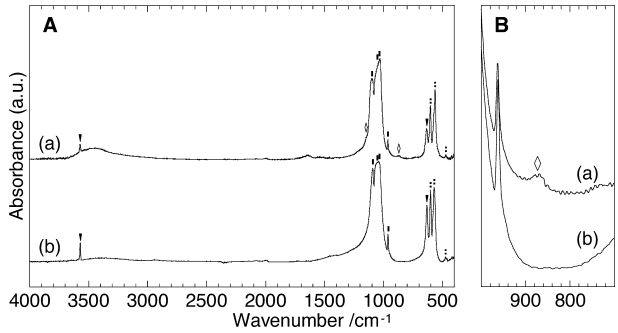

Fig. 3. IR spectra of (a) as-deposited HA whiskers and (b) as-deposited HA powders; A) the patterns in wide wavenumber range of 400–4000 cm^{-1} and B) the magnified patterns around 700–1000 cm^{-1}. The short solid lines and short dotted lines denote the peaks of PO_4^{3-} (stretching and bending modes) and the solid triangles and open rhombus denote the peaks of OH^- and HPO_4^{2-}, respectively.

HPO_4^{2-} ions in the whiskers. Actually, as a result of ICP-OES measurement, Ca/P molar ratios were calculated to be 1.53 for the whiskers and 1.63 for the powders. Considering these results, the ionic composition of the whiskers was calculated to be $Ca_{9.18}[HPO_4]_{0.82}[PO_4]_{5.18}[OH]_{1.18}{\cdot}n\ H_2O$ by assuming the following general formula for calcium-deficient HA:[15)–17)]

$$Ca_{10-z}[HPO_4]_z[PO_4]_{6-z}[OH]_{2-z}{\cdot}n\ H_2O\ (z = 0–1).$$

Although no IR absorption peaks of HPO_4^{2-} were detected, the powders also seemed to include a small calcium deficiency. The composition was calculated to be $Ca_{9.78}[HPO_4]_{0.22}[PO_4]_{5.78}[OH]_{1.78}{\cdot}n\ H_2O$. The OH^- content in the whiskers (1.18) corresponds to about 66 % of the content in the powders (1.78), and is in good agreement with the results of the IR measurements.

The thermogravimetric behavior of the HA whiskers and powders is shown in **Fig. 4**A, where x denotes molar water elimination per molar composition of $Ca_{10-z}[HPO_4]_z[PO_4]_{6-z}[OH]_{2-z}$ (z = 0.82 for whiskers and 0.22 for powders). It can be found that the total water eliminated from the whiskers was significantly greater than that from the powders. Based on the temperature differentiation of the thermogravimetric behavior, water elimination from the whiskers seems to progress through mostly four stages that occur in the temperature ranges of 25–250°C (peak maximum: 80°C), 250–400°C (peak maximum: 340°C), 400–600°C (peak maximum: 550°C), and 700–900°C (peak maximum: 790°C) (Fig. 4B). According to previous reports,[18)–20)] the first stage is the elimination of adsorbed water from the surface and fine pores. The significantly larger mass loss from the whiskers

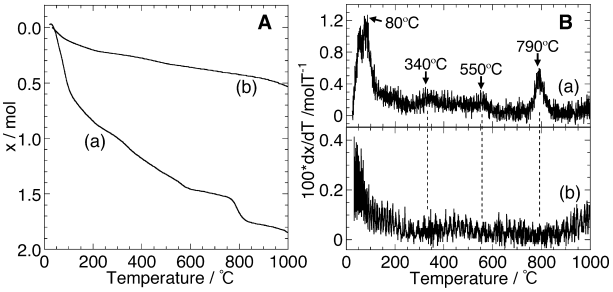

Fig. 4. Thermogravimetric behavior of water in (a) as-deposited HA whiskers and (b) as-deposited HA powders; A) accumulated amount of water eliminated with temperature and B) temperature differentiation of water elimination. The value x denotes molar water elimination per molar composition of whiskers and powders.

than from the powders at this stage is consistent with the results of IR measurement, in which the greater IR absorption by the adsorbed water (around 3000–3800 cm^{-1}) was detected in the whiskers compared with the powders. In contrast, it is known that calcium deficient HA has lower thermal stability than does stoichiometric HA and it decomposes into stoichiometric HA and β-tricalcium phosphate (TCP) via the following reaction: [17),21)]

$$Ca_{10-z}[HPO_4]_z[PO_4]_{6-z}[OH]_{2-z} \rightarrow$$

$$(1–z)\ Ca_{10}[PO_4]_6[OH]_2 + 3z\ Ca_3[PO_4]_2 + z\ H_2O.$$

In this reaction, the formation of β-TCP occurs around 700–900°C after HPO_4^{2-} is slowly converted into $P_2O_7^{4-}$ in the temperature range of 300–680°C accompanied by water elimination ($2\ HPO_4^{2-} \rightarrow P_2O_7^{4-} + H_2O$). By recognizing that the whiskers consisted of calcium-deficient HA, the loss of mass in the second and third stages is assumed to occur due to the conversion of HPO_4^{2-} into $P_2O_7^{4-}$. Decomposition from the intermediate compound including $P_2O_7^{4-}$ to HA and β-TCP takes place during the final stage:

$$Ca_{9.18}[HPO_4]_{0.82}[PO_4]_{5.18}[OH]_{1.18}$$

$$\rightarrow Ca_{9.18}[P_2O_7]_{0.41}[PO_4]_{5.18}[OH]_{1.18} + 0.41\ H_2O$$

(second and third stages)

$$\rightarrow 0.18\ Ca_{10}[PO_4]_6[OH]_2 + 2.46\ Ca_3[PO_4]_2 + 0.41\ H_2O$$

(final stage).

In the case of the powders, a very small loss of mass was observed in the temperature range of 300–680°C and no loss of mass was detected around 700–900°C. The observation indicates that the thermal stability of powders with small deficiencies is great enough to prevent thermal decomposition into β-TCP at temperatures below 1000°C.

3.2 Ion conduction property of HA whiskers

In **Figs. 5**A, B, C, and D, the typical impedance responses of the whisker compact (denoted by solid circles) and powder compact (denoted by open circles) at 250, 500, 600, and 850°C are shown as complex impedance plots with those of the sintered HA (denoted by open rhombi) as the reference. All plots consisted of a single semicircle described by a simple equivalent circuit of one capacitance and one resistance in parallel. Because the resistances of the crystalline grains and the grain boundaries were not separated, the conductivity was calculated by the total resistance of the grains and the grain boundaries. To eliminate

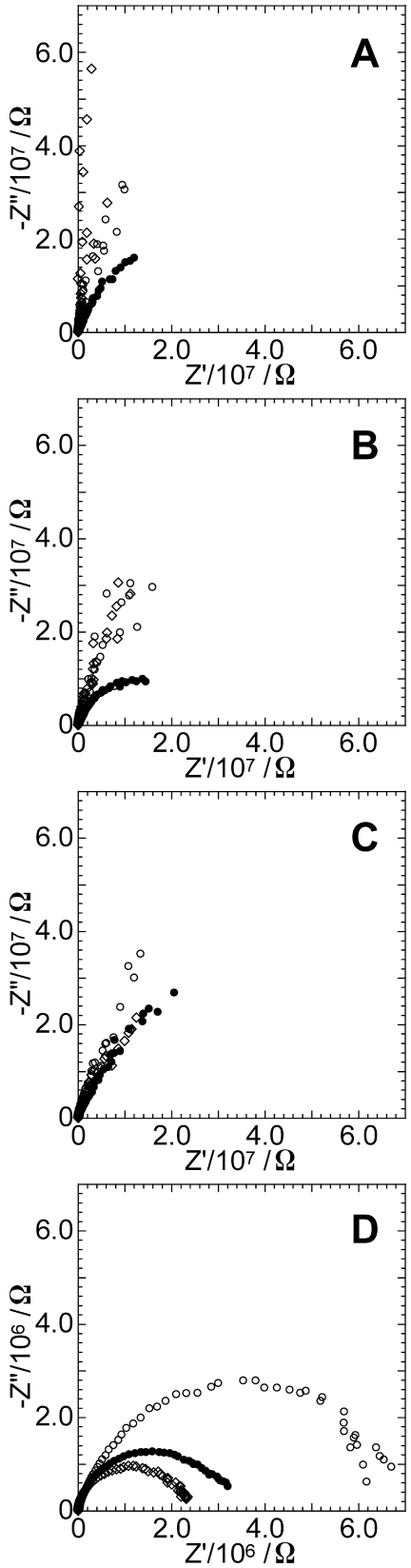

Fig. 5. Typical complex impedance plots of compacted HA whiskers, compacted HA powders, and sintered HA at A) 250°C, B) 500°C, C) 600°C, and D) 850°C. Solid and open circles denote the plots of compacted HA whiskers and powders, respectively, and open rhombus denote the plot of sintered HA.

the effects of void volume, the values were corrected by relative densities (whisker compact: 62% against $Ca_{9.18}[HPO_4]_{0.82}[PO_4]_{5.18}[OH]_{1.18}$, powder compact: 57% and sintered pellets: 96% against HA). The obtained conductivity is shown as the Arrhenius relationship (**Fig. 6**), showing that the three samples exhibited almost the same temperature dependence in the higher temperature range above 600°C. The linear increase of conductivity with the inverse of temperature is characteristic of the preferential ion conduction mechanism. As briefly described in the introduction section, conductivity in sintered HA has been reported to be the result of the migration of protons supplied by OH^- ions in the HA structure. The activation energy of the proton migration through OH^- ions in HA is a relatively higher value of around 1 eV,[1)] which shows good agreement not only with the activation energy of sintered HA in this study (1.03 eV) but also the values of the whisker compact (1.03 eV) and powder compact (1.09 eV) for temperatures above 600°C. This suggests that the conductivity of the whiskers and powders is also attributed to the protons in the OH^- ions in this temperature region. In contrast in the temperature range below 600°C, it is interesting to note that the non-linear temperature dependence of conductivity could be observed in the whiskers and powders, while the conductivity of the sintered HA was difficult to calculate because of the detection limit of the impedance. In particular, the whiskers showed the unique behavior that the conductivity once increased to around 5.0×10^{-9} S/cm and then decreased with temperature from 500 to 600°C. The conductivity of whiskers at 500°C was about one order of magnitude greater than powders at the same temperature and corresponded to the value of the whiskers at 700°C. It was assumed that the non-linear relationship probably came from the multiple ion migration mechanism.

3.3 Thermal change of HA whiskers after impedance measurements

Figure 7 shows SEM photographs of the surface of the compacted whiskers (a) and powders (b) before (1 in Figs. 7(a) and (b)) and after (2 in Figs. 7(a) and (b)) the impedance measurements. Because the non-linearity in the Arrhenius plot was observed below 600°C, the observation was also conducted for the surface after the measurement at 600°C (3 in Figs. 7(a) and (b)). As for the whisker compact, whisker shaped crystals (2–4 μm long and 0.1–0.3 μm wide) could be observed in both photographs 1 and 2 with no change in morphology after the measurement at 600°C. There seemed to be no relationship between conductivity and morphology. The smaller size of the whiskers than the as-deposited ones (see Fig. 1(a)) was probably caused by partial collapse of the grain under the high pressure while the compact was formed. In contrast, it was found that the morphology in Fig. 7(a)-3 was slightly different compared to Figs. 7(a)-1 and 2, suggesting that the morphology change from the anisotropic shape to the isotropic shape occurred during the temperature elevation from 600°C to 850°C. The Arrhenius plot of the whiskers, however, showed the linear relationship in this temperature region as described in the paragraph on the ion conductive properties. Considering this, proton conduction above 600°C probably occurred over a short distance within the crystal, which was little affected by changes in the sizes of the secondary particles. In the case of the powder compact, the morphology seemed not to change during the measurement from room temperature to 850°C.

The change of crystal structure in the samples after the impedance measurement was estimated by the XRD patterns of the surface of the whisker compact (**Fig. 8**(a)) and powder compact

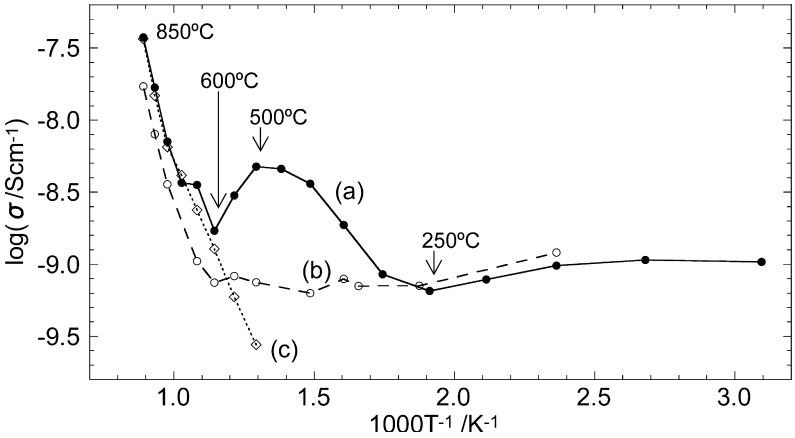

Fig. 6. Arrhenius plots of ionic conduction in (a) compacted HA whiskers, (b) compacted HA powders, and (c) sintered HA.

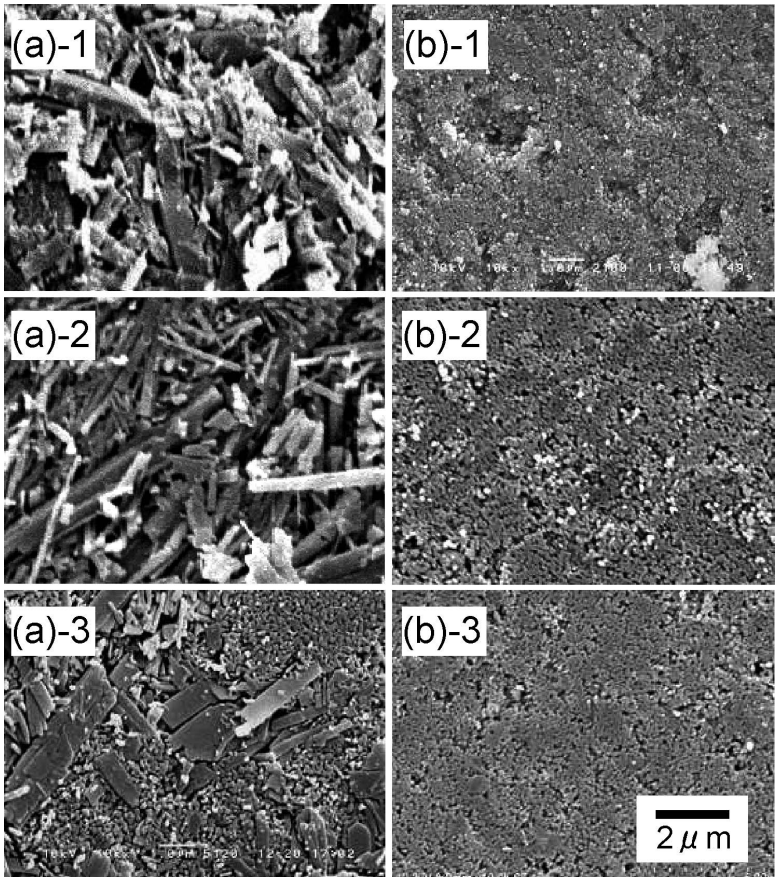

Fig. 7. SEM photographs of the surface of (a) compacted HA whiskers, (b) compacted HA powders, and (c) sintered HA. Photograph 1 represents the surface before impedance measurement and photographs 2 and 3 represent the surface after impedance measurement at 600°C and 850°C, respectively.

(Fig. 8(b)). 1, 2, and 3 correspond to the patterns before the impedance measurement, after the measurement at 600°C, and at 850°C, respectively. For reference, the patterns of the as-deposited samples (pattern 0) are shown in Fig. 8. Compared to Fig. 8(a)-0, the intensity of (002) diffraction in Figs. 8(a)-1, 2, and 3 drastically decreased instead of the increase in diffraction from (300). This was surely caused by the effect of preferred orientation of the whiskers on the surface of the compact. Similarly, the difference in relative intensity observed among Figs. 8(a)-1, 2, and 3 seems not to be the result of the structural change during the impedance measurement but to the difference in the condition of the preferred orientation from lot to lot introduced during formation of the compact. There were no obvious changes in the diffraction positions (2θ) that originated in HA among all whisker samples, whereas the additional peaks from β-TCP (denoted by solid cones) appeared only in Fig. 8(a)-3. Based on these results, it was assumed that the unique conductivity profile of whiskers below 600°C was not the result of a change of the

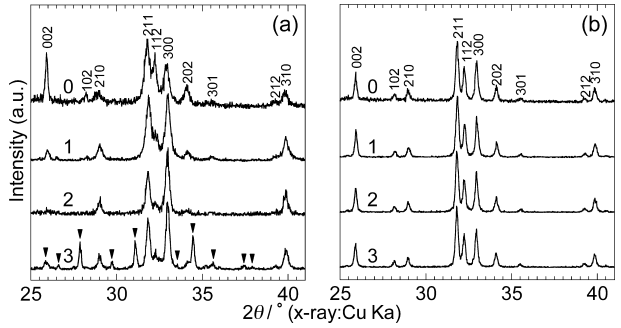

Fig. 8. XRD patterns of (a) HA whiskers and (b) HA powders. Pattern 0 represents the diffraction from as-deposited whiskers and powders, pattern 1 represents the diffraction from the surface of compacted samples before impedance measurement, and patterns 2 and 3 represent the surface of compacted samples after impedance measurement at 600°C and 850°C, respectively.

crystal structure, and the ion conduction mechanism above 600°C was free from the influence of β-TCP generation. As for the powder compact, there seemed to show no changes in peak position during the impedance measurement from room temperature to 850°C. The result also indicates that the presumed multiple mechanisms in conductivity below 600°C were not brought about by structural change.

Figures 9(a) and (b) are the IR patterns of the whiskers and powders before the impedance measurement (1), after the measurement at 600°C (2), and after the measurement at 850°C (3). During the temperature elevation from 600°C to 850°C, a significant change in the pattern attributable to the generation of β-TCP was observed in the whiskers. However, this change was considered as having no influence on proton migration in the HA crystal as judged by the linear relationship in the Arrhenius plot. In contrast, in the temperature range below 600°C, it was found that absorbance around 1030–1090 cm^{-1} (stretching mode of P–O bonds in PO_4^{3-} ion) sharpened slightly after the measurement

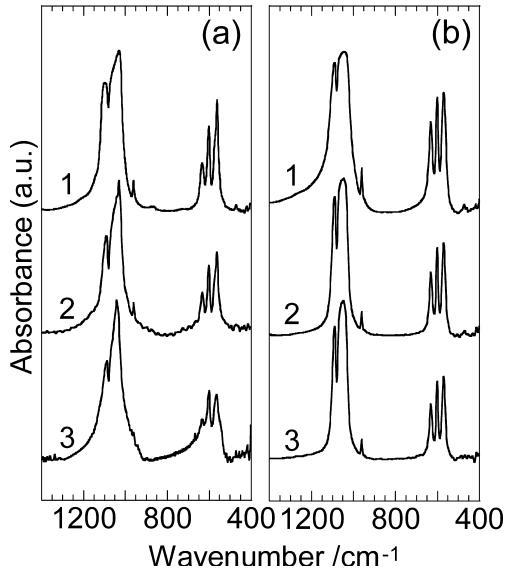

Fig. 9. IR spectra of (a) HA whiskers and (b) HA powders. Spectrum 1 represents IR absorption by samples before impedance measurement and spectra 2 and 3 represent IR absorption by samples after impedance measurement at 600°C and 850°C, respectively.

at 600°C in both the whisker and powder patterns. In addition, as for the whiskers, the absorption at 870 cm^{-1} that originated in HPO_4^{2-} disappeared after the measurement at 600°C. These results support the interpretation of mass loss in the TG curves (Fig. 4) that HPO_4^{2-} in the calcium-deficient HA converted into $P_2O_7^{4-}$ at the second and third stages (250–600°C). The drastic change in whisker conductivity was observed in almost the same temperature range from 250 to 600°C, indicating that the HPO_4^{2-} had a close correlation to the ion conduction in the whiskers. By plotting the TG curves on the Arrhenius plots of conductivity (**Fig. 10**), it was found that the conductivity changes are closely related to water elimination. In the temperature range low enough to allow the adsorbed water to exist on the surface, proton conduction is supposed to occur via the adsorbed water. This kind of surface conduction usually decreases with an increase in the temperature because the conduction path decreases with the elimination of adsorbed water, whereas the probability of generation of movable carriers increases with temperature. The apparent non-linear relationship between σ against $1/T$ below 250°C was probably caused by the binary interaction of the decreasing and increasing conduction through adsorbed water with temperature elevation. In contrast, based on the results of TG and IR measurements, the temperature range of 250–400°C corresponds to the second stage where the proton in HPO_4^{2-} has high mobility for conversion into $P_2O_7^{4-}$. The amount of water eliminated during the heating from 250°C to 400°C was estimated to be about x = 0.26 for the whiskers (Fig. 4A(a)). Since a value of x = 0.41 is obtained for the complete conversion from HPO_4^{2-} to $P_2O_7^{4-}$, it was considered that the protons were retained within the whiskers up to at least 400°C. By taking into account the existence of two main stages of the second and third stages during the conversion, suggestion of the following two-step reactions was possible:

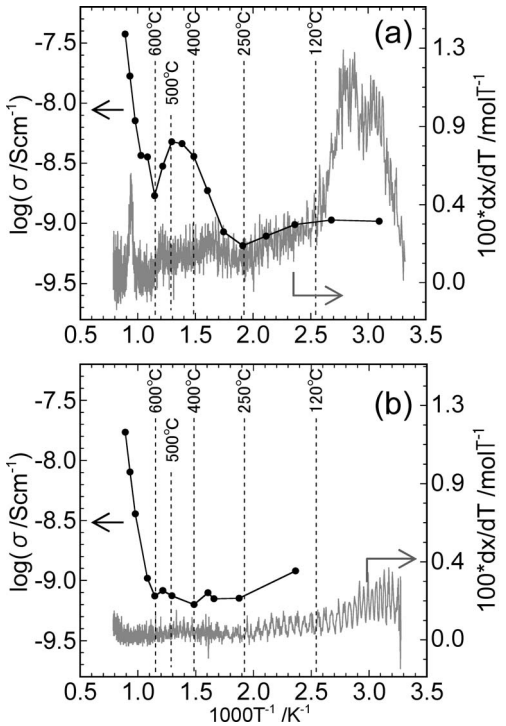

Fig. 10. Arrhenius plots of ionic conduction in (a) compacted HA whiskers and (b) compacted HA powders with the plots of temperature differentiation of water elimination from each sample against inverse temperature.

$$Ca_{9.18}[HPO_4]_{0.82}[PO_4]_{5.18}[OH]_{1.18}$$

$$\rightarrow Ca_{9.18}[P_2O_7]_{0.41}[PO_4]_{5.18}[OH^-]_{1.18+\delta}\,[H^+]_{\delta} + (0.41-\delta)\,H_2O$$

(second stage),

and

$$Ca_{9.18}[P_2O_7]_{0.41}[PO_4]_{5.18}[OH^-]_{1.18+\delta}\,[H^+]_{\delta}$$

$$\rightarrow Ca_{9.18}[P_2O_7]_{0.41}[PO_4]_{5.18}[OH]_{1.18} + \delta\,H_2O$$

(third stage).

The high conductivity at the second stage is presently attributed to the proton migration (δH^+) in the HA lattice. The subsequent decrease of conductivity at the third stage might result from the decrease in the number of protons generated with the water elimination. In the case of the powders, the same mechanism was basically supposed to cause the non-linear behavior in conductivity below 600°C, while the degree of change was much smaller than that in the whiskers.

4. Conclusion

HA whiskers synthesized via ACP were proved to be Ca-deficient HA with a Ca/P molar ratio of 1.53. The HPO_4^{2-} in the Ca-deficient whiskers was responsible for the high ionic conductivity in the temperature range of 250–600°C. Since the practical temperature for the poling of HA is 200–500°C based on our previous studies, the high ionic conduction below 600°C in Ca-deficient whiskers can be used for controlling the poling conditions. Furthermore, it seems to be possible to attain higher conductivity by controlling the concentration of HPO_4^{2-}. Because of the excellent selectivity in the adsorption of biological materials and electromagnetic functionalization, HA whiskers are expected to play an important role in the expansion of biomedical applications. The polarization properties of a series of Ca-deficient HA whiskers and the poling effect of HA whisker electrets on biological materials are currently being studied.

Acknowledgments This work was partly supported by a Grant-in-Aid from the Japan Society for the Promotion of Science (#19300169). Some of the authors (Y. T., M. N., and A. N.) would also like to express their thanks to "The Kazuchika Okura Memorial Foundation" for a grant for this research.

References

1) K. Yamashita, K. Kitagaki and T. Umegaki, *J. Am. Ceram. Soc.*, **78**[5], 1191–1197 (1995).
2) A. Obata, S. Nakamura and K. Yamashita, *Biomaterials*, **25**[21], 5163–5169 (2004).
3) M. Ueshima, S. Nakamura and K. Yamashita, *Adv. Mater.*, **14**[8], 591–595 (2002).
4) S. Nakamura, H. Takeda and K. Yamashita, *J. Appl. Phys.*, **89**[10], 5386–5392 (2001).
5) M. Nakamura, K. Niwa, S. Nakamura, Y. Sekijima and K. Yamashita, *J. Biomed. Mater. Res. B*, **82B**[1], 29–36 (2007).
6) S. Itoh, S. Nakamura, M. Nakamura, K. Shinomiya and K. Yamashita, *Biomaterials*, **27**[32], 5572–5579 (2006).
7) S. Nakamura, T. Kobayashi and K. Yamashita, *J. Biomed. Mater. Res. A*, **61**[4], 593–599 (2002).
8) T. Kobayashi, S. Nakamura and K. Yamashita, *J. Biomed. Mater. Res. A*, **57**[4], 477–484 (2001).
9) T. Kawasaki, *J. Chromatogr. A*, **544**[17], 147–184 (1991).
10) W. Suchanek, M. Yashima, M. Kakihana and M. Yoshimura, *J. Am. Ceram. Soc.*, **80**[11], 2805–2813 (1997).
11) T. Toyama, A. Oshima and T. Yasue, *J. Ceram. Soc. Japan*, **109**[3], 232–237 (2001) [in Japanese].
12) K. Ioku, S. Yamauchi, H. Fujimori, S. Goto and M. Yoshimura, *Solid State Ionics*, **151**[1–4], 147–150 (2002).
13) M. Aizawa, A. E. Porter, S. M. Best and W. Bonfield, *Key Eng. Mat. Bioceramics 16*, **254**[2], 915–918 (2004).
14) S. Koutsopoulos, *J. Biomed. Mater. Res. A*, **62**[4], 600–612 (2002).
15) M. Tamai, K. Sakamoto, S. Yamaguchi and A. Nakahira, *J. Ceram. Soc. Japan*, **113**[2], 131–134 (2005).
16) A. Siddharthanm, S. K. Seshadri and T. S. Sampath Kumar, *J. Mater. Sci. Mater. M.*, **15**, 1279–1284 (2004).
17) L. Winand, *Ann. Chim. France*, **6**[9–1], 941–& (1961).
18) A. Bianco, I. Cacciotti, M. Lombardi, L. Montanaro and G. Gusmano, *J. Therm. Anal. Calorim*, **88**[1], 237–243 (2007).
19) T. Wang, A. D. Reisel and E. Müller, *J. Eur. Ceram. Soc.*, **24**, 693–698 (2004).
20) H. F. Milhofer, V. Hlady, F. S. Baker, R. A. Beebe, N. W. Wikholm and J. S. Kittelberger, *J. Colloid Interf. Sci.*, **70**[1], 1–9 (1979).
21) A. Mortier, J. Lemaitre and P. G. Rouxhet, *Thrmochim. Acta*, **143**[15], 265–282 (1989).